

Combined Fluorine-18-FDG and Carbon-11-Methionine PET for Diagnosis of Tumors in Lung and Mediastinum

Otto S. Nettelbladt, Anders E. Sundin, Sven O. Valind, Gunnar R. Gustafsson, Kristina Lamberg, Bengt Långström and Eythor H. Björnsson

Departments of Lung Medicine and Diagnostic Radiology, Uppsala University PET-Centre, Department of Thoracic Surgery, Uppsala University, Uppsala, Sweden

We evaluated the value of PET using ^{18}F -fluorodeoxyglucose (FDG) and ^{11}C -methionine, individually or in combination, to distinguish malignant from benign tumors and to identify or exclude mediastinal metastases. **Methods:** Seventeen patients with a tumor in the lung or mediastinum were evaluated with ^{18}F -FDG and ^{11}C -methionine PET. For morphological comparison, we used CT, and all findings were confirmed by histology of surgical resection specimens ($n = 16$) or by cytology ($n = 1$). **Results:** All tumors were visualized equally well with both tracers, and there were no false-positive results. In 2 patients with a malignant tumor, coexisting pneumonia was correctly diagnosed as an inflammatory lesion because of its wedge-like shape. PET correctly excluded hilar invasion and mediastinal lymph node metastases in 10 of 14 patients with primary lung tumor. PET identified mediastinal metastases in 4 of 4 patients. CT failed to detect mediastinal tumor spread in 2 patients and gave a false-positive reading in 2 others. Significantly higher uptake (SUV) and transport rate (slope) values were obtained from malignant than benign lesions with both tracers. No major differences were seen in either the levels of significance or accuracy when the two tracers were compared. Slope values did not add further information to what was obtained with SUV. Density correction of SUV and slope values, to avoid the influence of surrounding air as well as tumor heterogeneity, increased these differences somewhat. Both tracers distinguished malignant from benign lesions with a 93% sensitivity and an accuracy of 89%–95%, but sensitivity improved to 100% when values from both tracers were combined. **Conclusion:** Fluorine-18-FDG and ^{11}C -methionine PET visualized all tumors equally well and detected mediastinal spread better than CT. For differentiation purposes, the problems of false-positive and false-negative PET findings could not be safely overcome in a limited number of cases either by the use of both tracers, by the additional use of slope values or by lesion density correction.

Key Words: PET; fluorine-18-fluorodeoxyglucose; carbon-11-methionine; lung tumor; mediastinal metastases; staging

J Nucl Med 1998; 39:640–647

Non-small cell lung cancer (NSCLC) has become a prime cause of death from malignant diseases (1). Most of the 12%–13% of patients with NSCLC who survive are nevertheless those with surgically resectable disease (2,3). To identify this potentially curable subgroup, thorough preoperative evaluation including invasive diagnostic operations is necessary. Unfortunately, these procedures are associated with patient morbidity and high cost (4) and are not particularly sensitive or specific (5–8). CT can identify a subgroup of benign (e.g., calcified) tumors, but many lesions remain indeterminate (9–13).

The introduction of PET has afforded a new approach to the

diagnosis of malignant diseases, including lung cancer (14). PET with ^{18}F -FDG has been shown in several reports to distinguish various types of lung cancer from benign lesions (15–20), though both false-positive and false-negative results can occur (21). Alternatively, the amino acid analog ^{11}C -methionine has been used, with generally similar results (22–25).

In previous studies on the value of PET for the detection of malignant lung tumors, only one tracer, either ^{18}F -FDG or ^{11}C -methionine, has been evaluated in a single patient population and only standardized uptake values (SUV) have been used in most studies. Furthermore, SUV and transport rate of tracer accumulation, determined in a tumor region, apply to a tissue mass with an unknown degree of heterogeneity at the cellular level. The tumor region may include a variety of components, both viable and necrotic tumor cells, edematous fluid and so on. Additionally, in the lung, alveolar gas may also constitute part of the volume, and in smaller lesions regional values of tracer concentration can be more influenced by surrounding tissue due to the limited spatial resolution of the tomographic measurement. The contribution of alveolar gas is also reflected in the physical density in the region of interest because the density of a region containing air is reduced in proportion to the gas volume contained. In view of the direct proportionality between density and the absorption of 511 keV photons by the body, a tomographic map of density, expressed in grams per centimeter (3), can be obtained from the PET transmission measurement (26). Thus, particularly in smaller lesions, corrections for tissue heterogeneity and the influence of surrounding air may theoretically improve the accuracy of the PET measurements.

The purpose of this study was to assess the value of the combined use of ^{18}F -FDG and ^{11}C -methionine PET in the preoperative evaluation of patients with lung tumor. We also compared the value of SUV versus transport rate (slope) and considered whether density correction for partial volume effects would make PET quantification more accurate.

MATERIALS AND METHODS

Patient Selection

Seventeen patients [11 men, 6 women; aged 58 ± 12 yr (mean ± 1 s.d.); range 32–77 yr] scheduled for surgery of chest tumors were studied. With one exception (Case 1, Table 1, where only cytological investigation of bronchoscopic specimens was performed), biopsy specimens from both the primary tumor and hilar mediastinal metastases were obtained at surgery. The specimens were evaluated by routine histopathological procedures, and the diagnoses (Table 1) were not subsequently reconsidered in any case. None of the patients had been receiving any other therapy at the time of surgery/needle biopsy. Before PET, all patients had been assessed with conventional preoperative investigations, in-

Received Feb. 1, 1997; revision accepted Jun. 24, 1997.

For correspondence or reprints contact: Otto Nettelbladt, Department of Lung Medicine, Uppsala University, Akademiska Sjukhuset, S-751 85 Uppsala, Sweden.

TABLE 1
Patient Data, Lesion Characteristics and Surgical Occurrence of Mediastinal Metastases Compared with CT and PET

Patient no.	Age (yr)	Sex	Tumor location	Malignant/benign	Histology	Lesion size* (cm ²)	Tumor density† (g/cm ³)	Mediastinal metastasis		
								Surgically verified	On CT	On PET
1	77	M	Sin	Malignant	Squamous cell carcinoma	3.60	0.74	nd	Yes	Yes
2	62	M	Sin	Malignant	Large cell carcinoma	9.08	1.10	No	No	No
3	47	M	Sin	Malignant	Squamous cell carcinoma	4.68	1.04	No	No	No
4	70	M	Dx	Benign	Lung cyst	1.52	0.81	No	No	No
5	49	F	Med.	Benign	Cystic thymoma	9.66	1.01	No	No	No
6	67	M	Sin	Malignant	Large-cell carcinoma	2.66	0.75	No	No	No
7	43	F	Sin	Malignant	Adenocarcinoma	7.92	0.97	Yes	No	Yes
8	32	F	Med.	Malignant	Extraskelatal osteosarcoma	12.62	1.11	No	No	No
9	70	F	Dx	Malignant	Adenocarcinoma	4.33	0.85	No	No	No
10	56	F	Dx	Malignant	Adenocarcinoma	6.29	0.95	No	No	No
11	69	M	Sin	Malignant	Squamous cell carcinoma	6.16	0.98	No	Yes	No
12	66	M	Sin	Malignant	Rectal adenocarcinoma‡	5.90	0.98	No	No	No
13	70	M	Sin	Malignant	Squamous cell carcinoma	7.69	1.03	Yes	Yes	Yes
14	47	M	Sin	Malignant	Adenocarcinoma	21.68	1.10	No [§]	No [§]	No [§]
15	48	F	Dx	Malignant	Adenosquamous carcinoma	4.60	0.89	No	Yes	No
16	64	M	Dx	Malignant	Squamous cell carcinoma	13.76	1.03	Yes	No	Yes
17	53	M	Sin	Malignant	Adenocarcinoma	2.60	0.57	No	No	No

* Mean from ¹⁸F-FDG and ¹¹C-methionine PET.

† Attenuation measurement in connection with PET.

‡ Lung metastasis of rectal adenocarcinoma.

§ Surgically verified contralateral lung metastasis in this patient detected by CT and ¹⁸F-FDG-PET but not included in the axial field of view of the camera at ¹¹C-methionine-PET.

M = male; F = female; nd = not done; Sin = left lung; Dx = right lung; Med. = mediastinal origin.

cluding CT, lung function tests and bronchoscopic or transthoracic biopsies. Fifteen patients had a malignant tumor, and two had a benign lesion (Table 1). One patient (Case 12) was later found to have metastases from a rectal carcinoma; all other patients had primary thoracic lesions. In two patients with lung cancer, coexisting pneumonia was found. All 17 patients were investigated with both tracers. The surgical decision was made independently of the PET results. The study was approved by the Ethical Committee of the Medical Faculty of Uppsala University, and all patients gave their informed consent.

PET

The ¹¹C and ¹⁸F were produced at the Uppsala University PET Center. The ¹¹C was produced as ¹¹CO₂ by the ¹⁴N(p,α)¹¹C reaction using a Scanditronix 17 MeV cyclotron (Scanditronix AB, Uppsala, Sweden). Carbon-11-methionine was synthesized via ¹¹C-methyl iodide and prepared for intravenous administration (27). Fluorine-18-FDG was synthesized according to a previously described method using a PETtrace FDG MicroLab system (General Electric Medical Systems, Uppsala, Sweden) (28).

The patients were examined with a Scanditronix GE 4096 whole-body PET camera that simultaneously produces 15 contiguous, 6.5-mm-thick axial slices and an in-plane resolution of 5–6 mm (29). All patients fasted for at least 4 hr before undergoing PET examination. CT images or plain chest radiographs were used as a means to position the patient's tumor region in the axial field of view of the PET scanner. After a 10-min transmission scan at each of one or two bed positions, the tumor region was investigated after a rapid intravenous injection of (mean ± s.d.) 770 ± 100 MBq ¹¹C-methionine or 400 ± 70 MBq ¹⁸F-FDG. When the injection was started, a dynamic scanning sequence was initiated, continuing for 45 min (¹¹C-methionine) or 50 min (¹⁸F-FDG). When the main tumor was not located in the vicinity of the hilar regions, a second 10-min emission scan was performed to include these areas. Plasma samples from a peripheral vein in the foot, which was arterialized by warming, were obtained at scheduled

intervals and analyzed for ¹¹C or ¹⁸F concentration. The concentrations of blood glucose and plasma methionine were also measured.

Image Reconstruction and Analysis

The image reconstruction produced a set of dynamic images, each representing a quantitative estimate of the radioactivity concentration. A 128 × 128 matrix and a 6-mm Hanning filter were used. Data were corrected for attenuation and radiation scatter. The data obtained 14–45 min (¹¹C-methionine) or 35–50 min (¹⁸F-FDG) after injection were summed to produce an average image. The radioactivity concentration in the average image was recalculated to provide images of SUV.

Quantitative analyses were also performed on a pixel by pixel basis, according to the technique described by Patlak (30) generating images of transport rates (slope values) into tissues by using plasma radioactivity as a reference. Due to the paucity of individual analyses of plasma methionine metabolites, a standard correction was calculated from previous data (31).

In the SUV images, regions of interest (ROIs) representing the largest axial tumor area were drawn according to a standardized procedure whereby an isocontour was positioned halfway between the greatest tumor radioactivity and the adjacent areas. Thus, for each PET study, the Sokolow color scale was adjusted to 100% (white) for the area of the greatest tumor activity and 0% (black) for the region close to the tumor edge. The isocontour was then drawn along the 50% activity level. In each tumor ROI, an additional area comprising the four contiguous pixels (1.00 cm²) with the greatest activity and designated hotspot (hs) was identified. The ROIs in the SUV images (SUV, SUV_{hs}) were used in the transport rate images (slope, slope_{hs}). Moreover, thoracic vertebral bodies were outlined, and larger ROIs were drawn in normal lung, chest muscle and mediastinum at a level cranial to the heart.

All ROIs were also transferred from the SUV images to the corresponding transmission scans for measurements of attenuation. The latter were used to correct the indices of tumor tracer

TABLE 2
Individual SUV, Slope, SUV_{corr hs} and Slope_{corr hs} Values at Fluorine-18-FDG and Carbon-11-Methionine PET

Patient no.	Malignant/benign	¹⁸ F-FDG				¹¹ C-methionine			
		SUV	Slope	SUV _{corr hs}	Slope _{corr hs}	SUV	Slope	SUV _{corr hs}	Slope _{corr hs}
1	Malignant	10.5	5.5	16.9	9.2	4.6	4.9	7.0	8.3
2	Malignant	7.7	4.8	8.3	5.6	5.8	11.3	7.6	15.1
3	Malignant	7.9	4.4	8.4	4.8	5.6	10.8	7.1	14.1
4	Benign	2.6	0.9	3.3	1.0	2.9	4.7	4.0	6.8
5	Benign	2.3	0.6	2.5	0.7	1.7	2.4	2.4	3.0
6	Malignant	2.3	0.9	3.3	1.4	4.1	4.7	6.5	7.5
7	Malignant	8.9	4.2	12.0	6.2	5.4	7.7	6.6	9.6
8	Malignant	5.8	3.2	7.2	4.1	7.5	17.7	8.4	19.5
9	Malignant	4.8	3.2	7.7	5.3	2.8	4.9	3.5	6.4
10	Malignant	3.4	1.5	4.0	1.8	5.3	12.8	7.0	16.9
11	Malignant	9.0	3.7	11.8	5.2	8.5	11.5	10.7	14.4
12	Malignant	8.5	4.8	10.3	6.0	4.9	8.2	6.6	11.5
13	Malignant	8.1	4.8	9.4	5.7	5.8	9.0	7.3	11.2
14	Malignant	8.7	5.9	9.7	6.7	6.7	15.1	8.4	15.7
15	Malignant	4.9	2.8	6.2	3.6	3.9	7.1	6.0	10.9
16	Malignant	15.8	7.7	20.3	11.5	9.6	10.5	11.3	12.5
17	Malignant	3.0	1.3	7.2	2.9	3.8	6.1	6.9	11.0
3*	Benign (pneumonia)	3.2	1.3	1.1	1.5	3.7	6.9	4.5	8.3
7*	Benign (pneumonia)	3.3	1.4	5.2	2.4	3.4	4.3	7.7	9.9

* Patients 3 and 7 also had pneumonia, distinctly separate from their primary tumor.

Patients are numbered as in Table 1.

nd = not done.

accumulation for variations in density. The tumor tissue density was calculated by multiplying the ratio of the attenuation in the lesion and mediastinum by the density of mediastinum (1.04) according to Rhodes et al. (26). The density-corrected indices were then obtained by dividing the tumor SUV and slope value, respectively, by the lesion density. The values obtained (SUV_{corr}, slope_{corr} and SUV_{corr hs}, slope_{corr hs}, respectively) were thus expressed relative to the air-free tissue content of the lesion rather than relative to the thoracic volume occupied by the lesion. In addition, corrected tracer accumulation values were calculated for the two pneumonias.

CT

Intravenous contrast-enhanced CT was performed during sustained respiration with a Siemens Somatom Plus or AR CT scanner (Siemens, Erlangen, Germany) using 8- or 10-mm slice thickness and increment. Scanning parameters were 130 or 140 kV, 130 or 200 mAs. Images were reconstructed by standard algorithms. In four of the patients, spiral CT was applied. A 17.2-cm scan including the hilar regions and the upper or lower thorax, depending on the previous findings on chest radiographs, was performed during 24 s at 137 kV and 110 mAs and reconstructed in 8-mm overlapping slices with 4-mm increment.

Image Interpretation

The CT images were interpreted blind by a board-certified thoracic radiologist. In the vast majority of patients, the PET examinations were performed by one physician, and the images were then analyzed by another board-certified radiologist trained in PET who was blind to both the results of CT and chest radiography and the surgical and histopathological findings. The PET imaging reports, written separately for ¹¹C-methionine and ¹⁸F-FDG described the location of the lesions and the presence or absence of metastases. At the final image evaluation, PET and CT were viewed together retrospectively. The results of PET and CT were correlated to the findings at surgery. In this prospective study, the

surgical decision was taken independently from the PET results. Surgery was therefore performed even in cases where additional lesions were diagnosed by PET, thereby leading to an upstaging of the disease.

Statistical Analysis

Nonparametric Mann-Whitney U tests and Wilcoxon signed rank tests were used for unpaired and paired analyses, respectively. In calculations of sensitivity and specificity, optimal cutoffs were chosen retrospectively for each tracer SUV_{corr hs} and slope_{corr hs} value to yield the fewest false-negative and false-positive cases possible. Pneumonia was found in two patients with malignant primary lesions. Because pneumonia is known to have critically indeterminate PET values, in the absence of any existing case with only pneumonia as a primary lesion, these lesions have been statistically evaluated as separate cases. In contrast, mediastinal metastases of a primary lung tumor, already included in the calculations, were not evaluated separately.

RESULTS

All individual patient characteristics, including histopathological results and the occurrence of metastases at surgery, CT and PET are reported in Table 1. The individual quantitative PET results are given in Table 2.

CT

In comparison with the operative findings, CT correctly located the lung tumors in 15 patients and located the mediastinal tumors in the remaining two patients. CT correctly excluded tumor growth from the lung into the mediastinum or the presence of pathologically enlarged hilar and/or mediastinal lymph nodes (short axial diameter >1 cm) in 8 of 14 patients with primary lung tumors. In the remaining six patients, mediastinal CT findings were shown to be false-positive in two, true-positive in one, false-negative in two and not confirmed in the unoperated patient. Contralateral lung metastases were suspected at CT in one patient with adenocarci-

noma (Case 14, Table 1). Lung opacities, consistent with bronchopneumonia and confirmed by surgery, were found to coexist with but were distinctly separate from the tumor in two patients.

PET—Visual Evaluation

Fluorine-18-FDG PET and ^{11}C -methionine PET detected all the 15 lung and two mediastinal tumors equally well. The pattern of tracer accumulation was the same for both ^{11}C -methionine and ^{18}F -FDG where most lesions were visualized as focal areas of increased tracer accumulation in comparison with the surrounding tissues (Fig. 1). In the larger tumors, however, a central region of low radioactivity concentration was found (Fig. 2) corresponding to tumor necrosis. In one patient with a cystic tumor (a benign thymoma), the tracer accumulated exclusively in a thin peripheral rim of solid tissue (Case 5, Table 1, Fig. 3). A benign lung cyst (Case 4, Table 1) was faintly visible at PET but was found quantitatively to have an unexpectedly high tracer accumulation with both tracers (Table 2).

PET with both tracers correctly and independently excluded hilar invasion and mediastinal lymph node metastases in 10 of 14 patients with primary lung tumor. PET with both tracers detected mediastinal tumor spread later confirmed by surgery in the three patients as well as in the patient who didn't undergo surgery (Case 1, Table 1, Fig. 1). Visual evaluation with ^{18}F -FDG PET also detected contralateral lung metastases near the right diaphragm in Case 14 (Table 1), but this area was not included in the axial field of view with ^{11}C -methionine PET. In two patients with lung cancer (Cases 3 and 7, Table 1), pneumonia was also correctly diagnosed as an inflammatory lesion because of its wedge-like shape.

In the case of ^{11}C -methionine PET, small mediastinal areas of unspecific (nontumor) tracer accumulation were found in the occasional patient. These uptakes were rather confusing in the initial phase of the image reading, but they were found consistently to have a typical location corresponding to the mucous membranes of the carina and the proximal main bronchi, and could in the subsequent evaluation be discarded as nonspecific findings. On the other hand, the normal tissue uptake of ^{11}C -methionine by bone marrow and esophagus provided excellent anatomical landmarks that facilitated the image interpretation and made possible a more precise description of the tumor location (Fig. 4) than was the case with ^{18}F -FDG, where the normal tissue uptake was low.

PET—Quantitative Tissue Measurements

The variations in blood glucose and plasma methionine concentration were small (mean \pm s.d.) 4.8 ± 0.9 (range: 3.9–7.6) mmol/liter and 20 ± 5.8 (range: 11–33) μmol /liter, respectively.

Fluorine-18-FDG versus Carbon-11-Methionine. The uptake (SUV) and transport rate (slope) in tumors and normal tissues are given in Tables 2 and 3. In the tumors, including pneumonias, ^{18}F -FDG $\text{SUV}_{\text{corr hs}}$ values were higher than corresponding ^{11}C -methionine values (19% higher mean value, not significant). By contrast, the tumor transport rate ($\text{slope}_{\text{corr hs}}$) showed a converse relationship, with higher values for ^{11}C -methionine than for ^{18}F -FDG (148% higher mean value, $p < 0.001$). A weak correlation was found between the $\text{SUV}_{\text{corr hs}}$ for the two tracers ($r = 0.66$) but not between corresponding $\text{slope}_{\text{corr hs}}$. The tracer accumulation in the primary tumors did not differ significantly from that in the metastases, although there was a tendency toward higher values in the former.

Fluorine-18-FDG-PET. The tumor $\text{SUV}_{\text{corr hs}}$ and $\text{slope}_{\text{corr hs}}$ were closely correlated ($r = 0.97$). In the lung tumors, both $\text{SUV}_{\text{corr hs}}$ and $\text{slope}_{\text{corr hs}}$ were (mean 29% and 38%, respectively) higher than the corresponding uncorrected values ($p = 0.001$).

The density corrected values ($\text{SUV}_{\text{corr hs}}$, $\text{slope}_{\text{corr hs}}$) distinguished the benign from the malignant tumors irrespective of whether the pneumonias were included in the benign group ($p <$

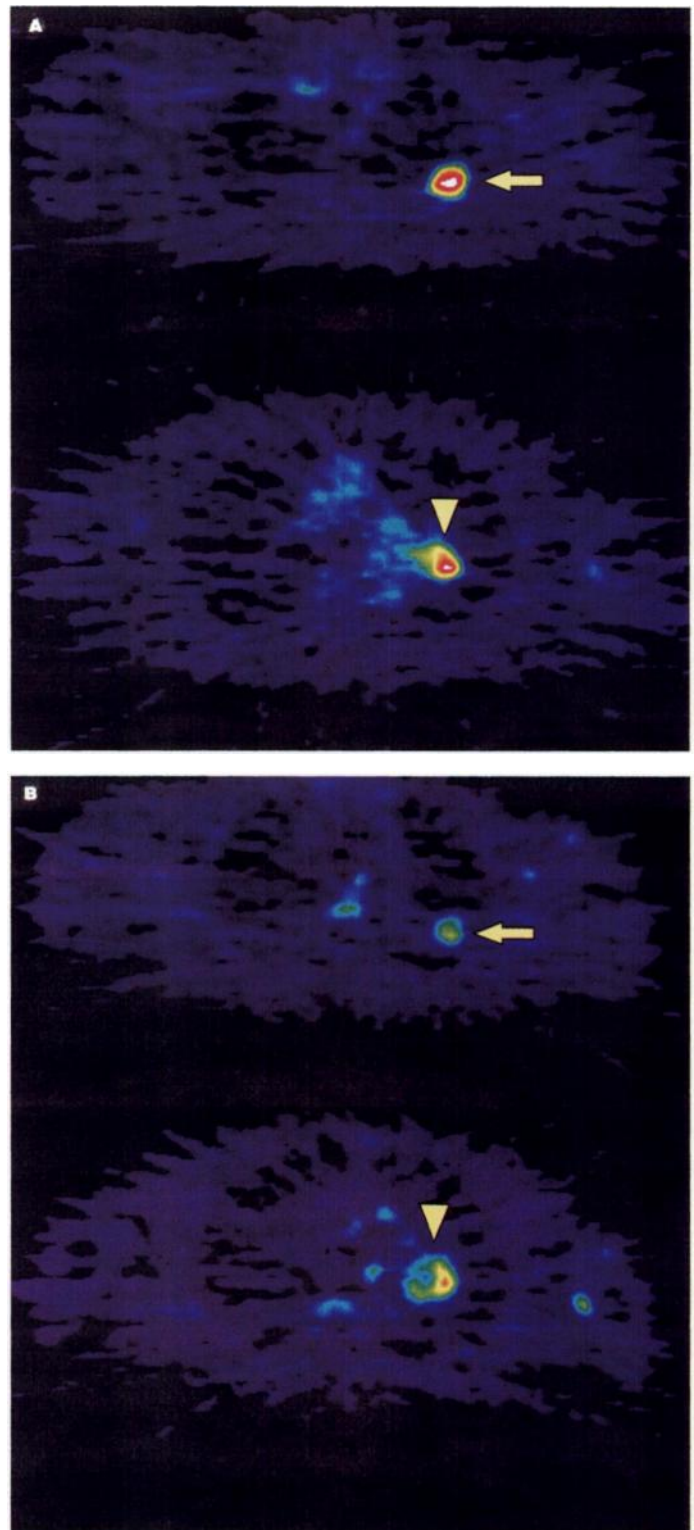


FIGURE 1. (A) Fluorine-18-FDG PET scan of a patient (Case 1, Table 1) with squamous cell carcinoma. Upper panel (arrows): lung tumor. Lower panel (arrow heads): mediastinal metastasis. (B) The same tumor and mediastinal metastasis as in (1A) visualized with ^{11}C -methionine PET.

0.01, $p < 0.01$) or not ($p < 0.05$, $p < 0.05$) (Table 3A). The levels of significance were decreased when uncorrected SUV (but not slope) was used (Table 3A).

When malignant tumors were compared with all nonmalignant lesions (the benign tumors plus the two pneumonias in Cases 3 and 7, Table 1), both $\text{SUV}_{\text{corr hs}}$ and $\text{slope}_{\text{corr hs}}$, with cutoffs of 3.5 and 1.5, respectively, correctly distinguished 14 of 15 malignant and 3 of 4 benign lesions, leaving one false-positive (pneumonia in

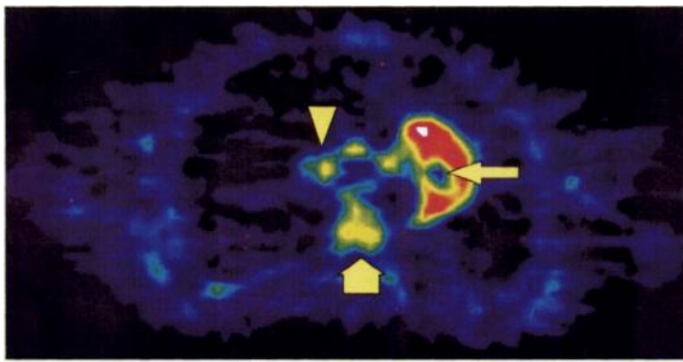


FIGURE 2. Carbon-11-methionine (right) PET of a patient (Case 13, Table 1) with squamous cell carcinoma with a central necrosis (arrow). Note the unspecific tracer accumulation corresponding to the carinal region and main bronchi (arrow head). Anatomical landmarks such as vertebral body (thick arrow) sternum and scapulae are easily identified.

patient 7, Table 1) and one false-negative case (large cell cancer in patient 6) (Fig. 5, Table 4). Thus, the sensitivity of both $SUV_{corr\ hs}$ and $slope_{corr\ hs}$ was 93%, the specificity 75% and the accuracy 89% (17 of 19).

For the uncorrected slope, similar values were obtained; but for SUV, sensitivity decreased to 87% (13 of 15) and accuracy to 84% (16 of 19), whereas specificity remained the same (Table 4).

Carbon-11-Methionine PET. A weak correlation was observed between tumor $SUV_{corr\ hs}$ and $slope_{corr\ hs}$ ($r = 0.71$). Mean tumor $SUV_{corr\ hs}$ and $slope_{corr\ hs}$ were both 40% higher than the corresponding uncorrected values ($p < 0.001$).

Carbon-11-methionine uncorrected SUV and slope distinguished significantly the benign from the malignant tumors, irrespective of

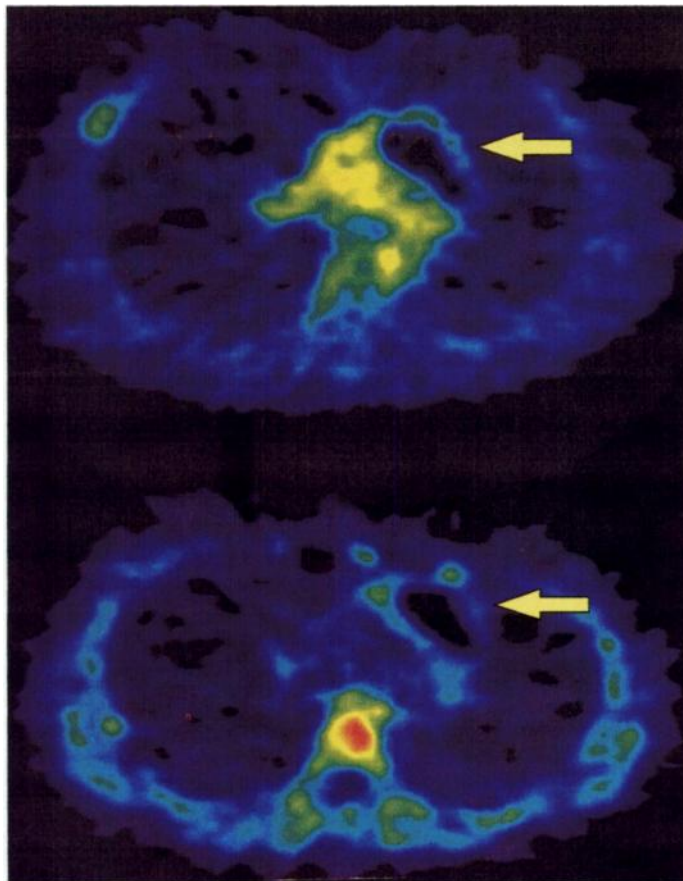


FIGURE 3. Fluorine-18-FDG (upper panel) and ^{11}C -methionine (lower panel) PET of a patient (Case 5, Table 1) with a cystic (benign) thymoma (arrow). Note the faint tracer accumulation in a thin peripheral rim of solid tissue.

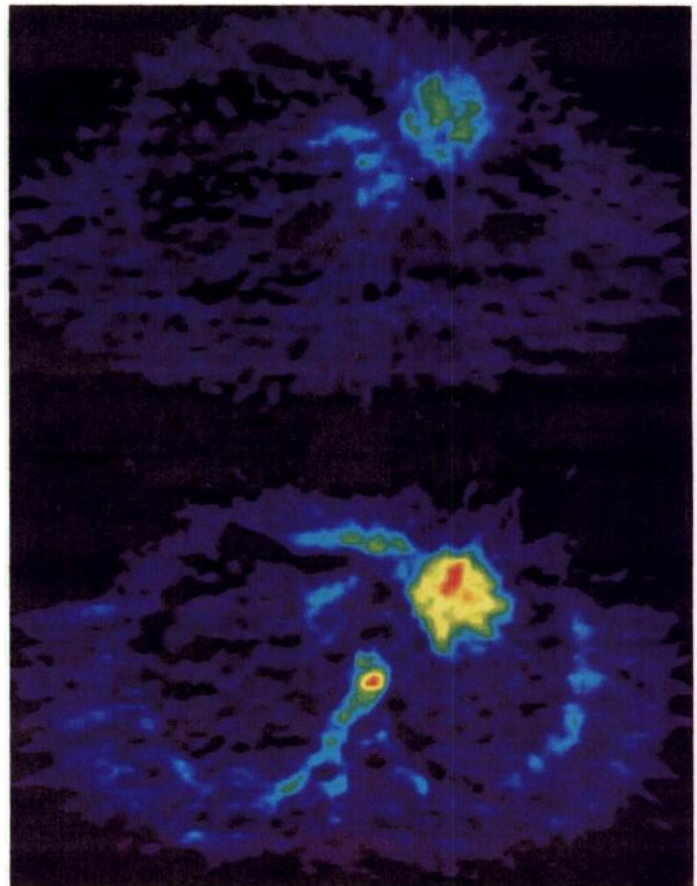


FIGURE 4. Fluorine-18-FDG (upper panel) and ^{11}C -methionine (lower panel) PET of a pneumonia in patient (Case 3, Table 1) with a central squamous cell carcinoma (not shown) with bronchial obstruction. Note the greater tracer accumulation of ^{11}C -methionine than of ^{18}F -FDG.

whether the pneumonias were included in the benign group ($p < 0.01$, $p < 0.05$) or not ($p < 0.05$ for both) (Table 3B). However, in contrast to corresponding ^{18}F -FDG values, only the $slope_{corr\ hs}$ (but not the $SUV_{corr\ hs}$) distinguished malignant from benign lesions, including pneumonias ($p < 0.05$), whereas both indices distinguished malignant and benign lesions equally well ($p < 0.05$ for both), provided the pneumonias were excluded (Table 3B).

With a cutoff of 5.0, uncorrected SUV distinguished 14 of 15 malignant tumors and 4 of 4 nonmalignant lesions (benign and pneumonias); sensitivity of 93%, specificity of 100% and accuracy of 95% in (18 of 19), whereas slope and $slope_{corr\ hs}$ incorrectly classified both cases of pneumonia above the cutoff (7.0), resulting in an equal sensitivity of 93% (14 of 15) but an impaired specificity of 50% (2 of 4) and an impaired accuracy of 84% (16 of 19) (Fig. 5, Table 4). For $SUV_{corr\ hs}$, sensitivity was unchanged, compared with uncorrected SUV, but specificity declined to 75% (3 of 4), giving an accuracy of 89% (17 of 19) (Fig 5, Table 4).

Combined ^{18}F -FDG and ^{11}C -Methionine Analysis. The combined analysis—including ranked values of indices from both tracers—distinguished malignant from benign lesions just as well as did the individual tracers ($p < 0.01$ and $p < 0.05$ for $SUV_{corr\ hs}$ and $slope_{corr\ hs}$, respectively; $p < 0.05$ for both uncorrected SUV and slope). When a lesion was considered malignant, provided either the ^{18}F -FDG or the ^{11}C -methionine value was above the cutoff limit chosen for the individual tracer, 15 of 15 malignant and 3 of 4 benign lesions were correctly identified with $SUV_{corr\ hs}$ (sensitivity of 100% in 15 of 15, specificity of 75% in 3 of 4 and accuracy of 95% in 18 of 19) (Fig. 5, Table 4). In the same fashion, $slope_{corr\ hs}$ had an equal 100% sensitivity (15 of 15) but was less specific 50% (2 of 4) and less accurate 89% (17 of 19) (Fig. 5,

TABLE 3
A: Fluorine-18-FDG PET Measurements (mean \pm 1 s.d.) for Different Tissues

Tissue	n	SUV	Slope \times $10^{-2}/\text{min}$	SUV _{corr}	Slope _{corr} \times $10^{-2}/\text{min}$	SUV _{hs}	Slope _{hs} \times $10^{-2}/\text{min}$	SUV _{corr hs}	Slope _{corr hs} \times $10^{-2}/\text{min}$
Tumors									
Benign	2	2.5 \pm 0.22	0.76 \pm 0.23	2.8 \pm 0.8	0.89 \pm 0.44	2.7 \pm 0.1	0.79 \pm 0.05	2.9 \pm 0.6	0.90 \pm 0.21
Malignant	15	7.3 \pm 3.4 [†]	3.90 \pm 1.80 [‡]	8.2 \pm 3.6 [‡]	4.40 \pm 1.90 [‡]	8.9 \pm 4.4 [†]	5.1 \pm 2.6 [‡]	9.5 \pm 4.5 [‡]	5.30 \pm 2.60 [‡]
Pneumonia	2	3.3 \pm 0.1	1.30 \pm 0.09	4.4 \pm 1.9	1.80 \pm 0.84	3.6 \pm 0.1	1.70 \pm 0.03	3.1 \pm 2.9	2.00 \pm 0.59
Metastases [§]	5	6.0 \pm 3.1	3.60 \pm 1.90	8.2 \pm 2.0	5.00 \pm 2.10	7.0 \pm 3.9	3.20 \pm 1.40	8.2 \pm 2.5	4.10 \pm 1.50
Lung	17	0.53 \pm 0.2	0.07 \pm 0.04	2.4 \pm 0.3	0.32 \pm 0.16				
Mediastinum	17	2.4 \pm 0.3	0.23 \pm 0.11						
Muscle	17	0.72 \pm 0.2	0.16 \pm 0.09						
Vertebral body	17	2.0 \pm 0.6	0.73 \pm 0.34						
Liver	4	3.2 \pm 0.4	0.35 \pm 0.15						

B: Carbon-11-Methionine PET Measurements (mean \pm 1 s.d.) for Different Tissues

Tissue	n	SUV	Slope \times $10^{-2}/\text{min}$	SUV _{corr}	Slope _{corr} \times $10^{-2}/\text{min}$	SUV _{hs}	Slope _{hs} \times $10^{-2}/\text{min}$	SUV _{corr hs}	Slope _{corr hs} \times $10^{-2}/\text{min}$
Tumors									
Benign	2	2.3 \pm 0.9	3.60 \pm 1.60	2.8 \pm 1.5	4.40 \pm 2.70	2.8 \pm 0.6	4.20 \pm 1.80	3.1 \pm 1.0	4.90 \pm 2.70
Malignant	15	5.6 \pm 1.8 [‡]	9.50 \pm 3.80 [†]	6.3 \pm 1.3 [†]	10.5 \pm 3.00 [†]	7.1 \pm 2.5 [‡]	11.9 \pm 4.70 [†]	7.4 \pm 1.9 [*]	12.3 \pm 3.70 [†]
Pneumonia	2	3.5 \pm 0.3	5.60 \pm 1.90	4.8 \pm 1.6	7.10 \pm 0.50	4.3 \pm 0.8	6.90 \pm 3.00	6.1 \pm 2.3	9.10 \pm 1.10
Metastases [§]	4	4.7 \pm 1.2	5.80 \pm 0.80	6.4 \pm 1.0	7.90 \pm 1.40	5.7 \pm 2.5	6.50 \pm 0.90	7.2 \pm 1.9	8.50 \pm 1.00
Lung	17	0.6 \pm 0.1	0.86 \pm 0.31	2.5 \pm 0.5	3.30 \pm 1.30				
Mediastinum	17	1.1 \pm 0.3	1.10 \pm 0.58						
Muscle	17	0.74 \pm 0.11	1.10 \pm 0.35						
Vertebral body	17	4.2 \pm 1.3	6.90 \pm 2.80						
Liver	4	11.2 \pm 2.2	17.8 \pm 5.80						

* p < 0.05 compared with benign tumors (n = 2).

† p < 0.05.

‡ p < 0.01 compared with benign tumors and pneumonias as a single group (n = 4).

§ Mediastinal metastases from lung cancer.

See Methods section for abbreviations of PET indices.

Table 4). Uncorrected SUV showed the same results as did SUV_{corr hs}. For uncorrected slope, sensitivity and accuracy decreased to 93% (14 of 15) and 84% (17 of 19), respectively, compared to Slope_{corr hs}, whereas the specificity remained the same (50%) (Table 4).

DISCUSSION

In this study, the diagnostic values of ¹⁸F-FDG and ¹¹C-methionine PET for lung tumors were investigated and compared. Visually, PET using either tracer detected all the malignant and benign tumors equally well. In contrast to CT, PET with either tracer correctly identified (and excluded) mediastinal lung cancer metastases. Significantly higher uptake and transport rate values were obtained in malignant than in benign lesions with both tracers. With optimally chosen cutoff limits, the uptake and transport rate values from either tracer distinguished malignant from benign lesions with a sensitivity of 87%–93% and an accuracy of 84%–95%. Sensitivity increased to 100% when both tracers were optimally combined.

The ability of PET to detect lung tumors and to distinguish between malignant and benign forms, as shown by the results of this study, confirms the findings in previous reports. Similar results have been obtained when using either ¹⁸F-FDG (15–20,32,33) or ¹¹C-methionine (24), where the levels of sensitivity to detect malignant lesions varied between 83% and 100%, and the specificities ranged between 60% and 100%. The false-negative cases were small tumors (17,19), adenocarcinomas (19,24,34), isolated cases of bronchioloalveolar cancer (34), liposarcoma (24), carcinoid (33) and recurrent bronchogenic carcinomas (32,35). The false-positive cases were mainly

inflammatory lesions such as abscesses (24,32), granulomas (17,19,24) and aspergillomas (19,24). In this study, an unexpectedly large accumulation of tracer was found in a lung cyst, although this lesion was visually interpreted as benign. Moreover, the relatively high tracer uptake found in the two cases of pneumonia did not hamper the visual interpretation, thanks to the wedge-like appearance of the lesions.

In one report, Kubota et al. (24) studied two different groups, either with ¹⁸F-FDG or with ¹¹C-methionine, but no patients were examined with both tracers. Generally speaking, when the two tracers were compared, we found that uptake values with ¹⁸F-FDG were somewhat higher, whereas transport rates were on average more than twice as high with ¹¹C-methionine. A correlation could be discerned between the ¹⁸F-FDG and ¹¹C-methionine SUV_{corr hs} but not between the corresponding slope_{corr hs}. No major differences were observed either in the degree of significance or in accuracy when the uptake and transport values of the two tracers were compared. With regard to the specificity data, reflecting the ability of PET to exclude malignancy, the paucity of benign lesions in this study must be taken into consideration when interpreting the results.

In the combined analysis of ¹⁸F-FDG and ¹¹C-methionine PET results, only a minor additional piece of information was forthcoming compared with what was found in the data from either individual tracer. This concerned the two false-negative cases of malignancy. The circumstance that categorized the lesion as malignant if it belonged to the malignant group by at

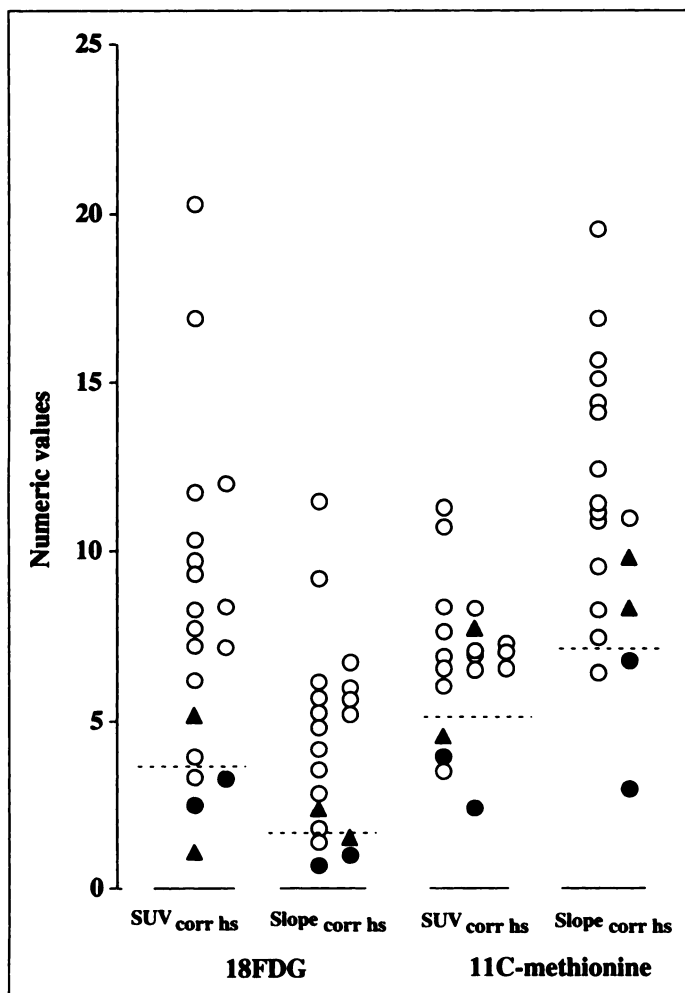


FIGURE 5. The distribution of individual $SUV_{corr\ hs}$ and $slope_{corr\ hs}$ ($\times 10^{-2}/min$) with PET using ^{18}F -FDG (two left groups) and ^{11}C -methionine (two right groups). Open circles are malignant lesions and filled circles and triangles represent benign tumors and pneumonias, respectively. Dotted lines are optimally chosen cutoffs.

least one of the tracers increased the sensitivity in the combined analysis to 100% for $SUV_{corr\ hs}$ and $slope_{corr\ hs}$. The specificity for $slope_{corr\ hs}$ was, however, reduced to 50%, that is, worse than for uncorrected ^{18}F -FDG slope, because both pneumonias would have been considered as malignant by the same criterion.

We found no advantage in distinguishing between malignant and benign lesions by adding transport rate (slope) values compared with uptake (SUV) values alone irrespective of whether these indices were corrected for potential tissue density heterogeneity and/or partial volume effects of surrounding lung

tissue or not. By contrast, Hübner et al. reported that transport rate values were more accurate than uptake indices for separating cancers from benign masses (32). The addition of density correction marginally improved the sensitivity with ^{18}F -FDG but decreased the specificity with ^{11}C -methionine PET (Table 4, $SUV_{corr\ hs}$ compared with uncorrected SUV), although these differences were due solely to the differences found in isolated cases (the tumor in Case 17 and the pneumonia in Case 3, Table 2).

The main problem with CT visualization of mediastinal lung cancer metastases is that the image reading is based on the identification of enlarged lymph nodes. Thus, metastases within the normal mediastinal node size range (largest diameter < 1 cm) usually escape detection. In a multi-institutional trial, Webb and colleagues found that, based on node size criteria, CT was 52% sensitive and 67% specific (11). Furthermore, McLoud et al. found that 40% of resected, visually enlarged nodes were free from cancer cells (36). In this study, where four patients had mediastinal metastases, CT detected only two of these cases, whereas two other CT scans were false-positive. In contrast, the visual interpretation of PET with both tracers correctly identified all four cases with mediastinal spread, but there were no false-positive mediastinal findings. Our findings are in agreement with an earlier study (37) in 11 patients with mediastinal involvement of NSCLC, where sensitivity and specificity values of 82% and 81%, respectively, were reported for ^{18}F -FDG-PET, compared with 64% and 44%, respectively, for CT.

CONCLUSION

The results of this article corroborate previous findings concerning the value of PET with ^{18}F -FDG and ^{11}C -methionine for tumor differentiation and the advantage of the technique over CT for staging of lung cancer. As in most other reports, an overlap between malignant and benign tumor accumulation indices was evident. The problem with these indeterminate lesions could not be fully overcome either by combined investigation with ^{18}F -FDG and ^{11}C -methionine or by the additional use of transport rate values or density correction for tumor heterogeneity and surrounding air.

ACKNOWLEDGMENTS

We thank Professor Gunnar Boman, Department of Lung Medicine; Associate Professor Per-Olof Osterman, Medical Superintendent, Department of Neurology; Dr. Lena Scheibenpflug and Dr. Wolfgang Kraaz, Department of Pathology, Uppsala University. We also thank Associate Professors Gunnar Hillerdal, Department of Lung Medicine, Karolinska Sjukhuset, Stockholm, Enn Nou, Department of Lung Medicine, Uppsala University and Göran Wegenius, Department of Diagnostic Radiology, Uppsala

TABLE 4
Sensitivity, Specificity and Accuracy of Separating Malignant from Benign Lung Tumors Using Various PET Indices

Measure	^{18}F -FDG				^{11}C -methionine				Combined ^{18}F -FDG and ^{11}C -methionine			
	SUV	$SUV_{corr\ hs}$	Slope	$slope_{corr\ hs}$	SUV	$SUV_{corr\ hs}$	Slope	$slope_{corr\ hs}$	SUV	$SUV_{corr\ hs}$	Slope	$slope_{corr\ hs}$
Sensitivity (%)	87 (13 of 15)	93 (14 of 15)	93 (14 of 15)	93 (14 of 15)	93 (14 of 15)	93 (14 of 15)	93 (14 of 15)	93 (14 of 15)	100 (15 of 15)	100 (15 of 15)	93 (14 of 15)	100 (15 of 15)
Specificity (%)	75 (3 of 4)	75 (3 of 4)	75 (3 of 4)	75 (3 of 4)	100 (4 of 4)	75 (3 of 4)	50 (2 of 4)	50 (2 of 4)	75 (3 of 4)	75 (3 of 4)	50 (2 of 4)	50 (2 of 4)
Accuracy (%)	84 (16 of 19)	89 (17 of 19)	89 (17 of 19)	89 (17 of 19)	95 (18 of 19)	89 (17 of 19)	84 (16 of 19)	84 (16 of 19)	95 (18 of 19)	95 (18 of 19)	84 (16 of 19)	89 (17 of 19)

Calculations for individual tracer (^{18}F -FDG and ^{11}C -methionine) and for the combined analysis are shown. In the combined data, a lesion was considered malignant if above cutoff with one tracer (see text and Fig. 1).

Ratios are shown within parentheses.

University for their advice and support. We thank Max Brandt for linguistic revision. This study received financial support from Akademiska Sjukhuset, Uppsala University, Uppsala, Sweden.

REFERENCES

1. Boring CC, Squires TS, Tong T, Montgomery S. Cancer statistics. *CA Cancer J Clin* 1994;44:7-26.
2. Jaklitsch M, Strauss G, Healey E, DeCamp M, Liptay M, Sugarbaker D. An historical perspective of multi-modality treatment for resectable non-small cell lung cancer. *Lung Cancer* 1995;12:S17-S32.
3. Non-small CLCG. Chemotherapy in non-small cell lung cancer: a meta-analysis using updated data on individual patients from 52 randomized clinical trials. *BMJ* 1995;311:899-909.
4. Williams A, Santiago S, Lehrman S, Popper R. Transcutaneous needle aspiration of solitary pulmonary masses: how many passes? *Am Rev Respir Dis* 1987;136:452-454.
5. Winning A, McIvor J, Seed WA, Husain O, Metaxas N. Interpretation of negative results in fine needle aspiration of discrete pulmonary lesions. *Thorax* 1986;41:875-879.
6. Wang K, Kelly S, Britt J. Percutaneous needle aspiration biopsy of chest lesions. New instrument and new technique. *Chest* 1988;93:993-997.
7. Schenk D, Bryan C, Bower J, Myers D. Transbronchial needle aspiration in the diagnosis of bronchogenic carcinoma. *Chest* 1987;92:83-85.
8. Polak J, Kubik A. Percutaneous thin needle biopsy of malignant and non-malignant thoracic lesions. *Radiologia Diagnostica* 1989;30:177-182.
9. Webb WR. Radiologic evaluation of the solitary pulmonary nodule. *Am J Roentgenol* 1990;154:701-708.
10. Scott WJ, Gobar LS, Hauser LG, Sunderland JJ, Dewan NA, Sugimoto JT. Detection of scalene lymph node metastases from lung cancer. Positron emission tomography. *Chest* 1995;107:1174-1176.
11. Webb WR, Gatsonis C, Zerhouni EA, et al. CT and MR imaging in staging non-small cell bronchogenic carcinoma: report of the Radiologic Diagnostic Oncology Group. *Radiology* 1991;178:705-713.
12. Swensen SJ, Morin RL, Schueler BA, et al. Solitary pulmonary nodule: CT evaluation of enhancement with iodinated contrast material—a preliminary report. *Radiology* 1992;182:343-347.
13. Bragg DG. Current applications of imaging procedures in the patient with lung cancer. *Int J Radiat Oncol Biol Phys* 1991;21:847-851.
14. Strauss LG, Conti PS. The applications of PET in clinical oncology. *J Nucl Med* 1991;32:623-648.
15. Wahl RL, Hutchins GD, Buchsbaum DJ, Liebert M, Grossman HB, Fisher S. Fluorine-18-2-deoxy-2-fluoro-D-glucose uptake into human tumor xenografts. Feasibility studies for cancer imaging with positron emission tomography. *Cancer* 1991;67:1544-1550.
16. Nolop K, Rhodes C, Brudin L, et al. Glucose utilization in vivo by human pulmonary neoplasms. *Cancer* 1987;60:2682-2689.
17. Scott WJ, Schwabe JL, Gupta NC, Dewan NA, Reeb SD, Sugimoto JT. Positron emission tomography of lung tumors and mediastinal lymph nodes using [¹⁸F]fluoro-deoxyglucose. The members of the PET lung tumor study group. *Ann Thorac Surg* 1994;58:698-703.
18. Abe Y, Matsuzawa T, Fujiwara T, et al. Clinical assessment of therapeutic effects on cancer using [¹⁸F]-2-fluoro-2-deoxy-D-glucose and positron and emission tomography: preliminary study of lung cancer. *Int J Radiat Oncol Biol Phys* 1990;19:1005-1010.
19. Slosman DO, Spiropoulos A, Couson F, et al. Satellite PET and lung cancer: a prospective study in surgical patients. *Nucl Med Commun* 1993;14:955-961.
20. Patz EF Jr, Lowe VJ, Hoffman JM, et al. Focal pulmonary abnormalities: evaluation with [¹⁸F]-fluorodeoxyglucose PET scanning. *Radiology* 1993;188:487-490.
21. Dewan NA, Gupta NC, Redepenning LS, Phalen JJ, Frick MP. Diagnostic efficacy of PET-F-FDG imaging in solitary pulmonary nodules. Potential role in evaluation and management. *Chest* 1993;104:997-1002.
22. Fujiwara T, Matsuzawa T, Kubota K, et al. Relationship between histologic type of primary lung cancer and carbon-11-L-methionine uptake with positron emission tomography. *J Nucl Med* 1989;30:33-37.
23. Kubota K, Matsuzawa T, Ito M, et al. Lung tumor imaging by positron emission tomography using [¹¹C]-L-methionine. *J Nucl Med* 1985;26:37-42.
24. Kubota K, Matsuzawa T, Fujiwara T, et al. Differential diagnosis of lung tumor with positron emission tomography: a prospective study. *J Nucl Med* 1990;31:1927-1932.
25. Kubota K, Yamada S, Ishiwata K, Ito M, Ido T. Positron emission tomography for treatment evaluation and recurrence detection compared with CT in long-term follow-up cases of lung cancer. *Clin Nucl Med* 1992;17:877-881.
26. Rhodes CG, Wollmer P, Fazio F, Jones TJ. Quantitative measurement of regional extravascular lung density using positron emission and transmission tomography. *J Comput Assist Tomogr* 1981;5:783-791.
27. Långström B, Antoni G, Gullberg P, et al. Synthesis of l- and d-[¹⁴C]methyl-¹¹C]methionine. *J Nucl Med* 1987;28:1037-1040.
28. Mulholland G, Toorongian S, Jewett D, Bachelor M, Kilbourn M. Routine production of 2-deoxy-2-[¹⁸F]fluoro-d-glucose by direct nucleophilic exchange on a quaternary 4-aminopyridinium resin. *Nucl Med Biol* 1990;17:273.
29. Kops E, Herzog H, Schmid A, Holte S, Feinendegen L. Performance characteristics of an eight-ring whole body PET scanner. *J Comput Assist Tomogr* 1990;14:437-445.
30. Patlak C, Blasberg R, Fenstermacher J. Graphic evaluation of blood-to-brain transfer constants from multiple-time uptake data. *J Cerebr Blood Flow Metab* 1983;3:1-7.
31. Hatazawa J, Ishiwata K, Itoh M, et al. Quantitative evaluation of L-[¹⁴C]methyl-¹¹C]-methionine uptake in tumor using positron emission tomography. *J Nucl Med* 1989;30:1809-1813.
32. Hübner KF, Buonocore E, Singh SK, Gould HR, Cotten DW. Characterization of chest masses by F-FDG positron emission tomography. *Clin Nucl Med* 1995;20:293-298.
33. Rege SD, Hoh CK, Glaspy JA, et al. Imaging of pulmonary mass lesions with whole-body positron emission tomography and fluorodeoxyglucose. *Cancer* 1993;72:82-90.
34. Dewan NA, Reeb SD, Gupta NC, Gobar LS, Scott WJ. PET-F-FDG imaging and transthoracic needle lung aspiration biopsy in evaluation of pulmonary lesions. A comparative risk-benefit analysis. *Chest* 1995;108:441-446.
35. Patz EF Jr, Lowe VJ, Hoffman JM, Paine SS, Harris LK, Goodman PC. Persistent or recurrent bronchogenic carcinoma: detection with PET and 2-[¹⁸F]-18]-2-deoxy-D-glucose. *Radiology* 1994;191:379-382.
36. McLoud TC, Bourgouin PM, Greenberg RW, et al. Bronchogenic carcinoma: analysis of staging in the mediastinum with CT by corrective lymph node mapping and sampling. *Radiology* 1991;182:319-323.
37. Wahl RL, Quint LE, Greenough RL, Meyer CR, White RI, Orringer MB. Staging of mediastinal non-small cell lung cancer with F-FDG PET, CT, and fusion images: preliminary prospective evaluation. *Radiology* 1994;191:371-377.

Iodine-131-Metaiodobenzylguanidine Uptake in Metastatic Carcinoid Tumor to the Orbit

Michael W. Hanson, Andrew M. Schneider, David S. Enterline, Jerome M. Feldman and Jon P. Gockerman
Division of Nuclear Medicine, Department of Radiology, Divisions of Endocrinology and Oncology, Department of Medicine, Duke University Medical Center, Durham, North Carolina

Metastatic tumor is one of several etiologies of space-occupying masses in the orbit that accounts for 1%-13% of all orbital masses (1). In the adult patient population, breast cancer is the most common tumor to metastasize to the orbit followed by metastases from the lung, prostate and gastrointestinal tract (2). It is rare for carcinoid tumors to metastasize to the eye or to the orbit. Carcinoid tumors arise from Kulchitsky cells that originate in the neural crest. Histologically, these tumors resemble, but are not as aggressive as, adenocarcinomas. Most carcinoids arise in the gastrointestinal tract

or the lung. The most common site for carcinoid metastases is the liver. On anatomical imaging studies, such as CT and magnetic resonance imaging, metastatic orbital carcinoid tumors appear as nonspecific tumor masses. Carcinoid tumors have an affinity for uptake of the radiopharmaceutical ¹³¹I-metaiodobenzylguanidine (MIBG) (3). We report a case of a patient with a known carcinoid tumor who developed a left orbital mass that demonstrated abnormal uptake of ¹³¹I-MIBG indicative of metastatic carcinoid tumor to the orbit.

Key Words: carcinoid tumor; orbital metastasis; iodine-131 metaiodobenzylguanidine

J Nucl Med 1998; 39:647-650

Received Dec. 16, 1996; revision accepted Apr. 14, 1997.
For correspondence or reprints contact: Michael W. Hanson, MD, Department of Radiology, Division of Nuclear Medicine, P.O. Box 3949, Duke University Medical Center, Durham, NC 27710.